Environmentally sensitive paramagnetic and diamagnetic contrast agents for Nuclear Magnetic Resonance Imaging and Spectroscopy

Jesus Paheco-Torres[1], Daniel Calle[1], Blanca Lizarbe[1], Viviana Negri[2], Carmen Ubide[2], Rosa Fayos[1], Pilar López Larrubia[1], Paloma Ballesteros[2] and Sebastian Cerdan[1*]

[1]Laboratorio de Imagen y Espectroscopía por Resonancia Magnética (LIERM), Instituto de Investigaciones Biomédicas "Alberto Sols" CSIC-UAM, c/ Arturo Duperier 4, Madrid 28029, Spain. [2]Laboratorio de Síntesis Orgánica e Imagen Molecular por Resonancia Magnética (SOIRM), Facultad de Ciencias, Universidad Nacional de Educación a Distancia, c/ Senda del Rey 9, Madrid 28040, Spain.

Running Title: Environmentally sensitive paramagnetic and diamagnetic probes

Correspondence: Prof. Sebastián Cerdán
Instituto de Investigaciones Biomédicas "Alberto Sols" CSIC/UAM.
c/ Arturo Duperier 4
Madrid 28029, Spain
Telf: 00-34- 91-585-4444
FAX: 00-34-91-585-4401
email: scerdan@iib.uam.es

(10745 words, 9 Figures)

Abstract: Even though alterations in the microenvironmental properties of tissues underlie the development of the most prevalent and morbid pathologies in developed countries, they are not directly observable in vivo by conventional Magnetic Resonance Imaging (MRI) or Spectroscopy (MRS) methods. This circumstance has lead to the development of a wide variety of exogenous paramagnetic and diamagnetic MRI and MRS probes able to inform non invasively on microenvironmental variables such as pH, pO_2, ion concentration o even temperature. This review covers the fundamentals of environmental contrast and the current arsenal of endogenous and exogenous MRI and MRS contrast enhancing agents available to visualize it. We begin describing briefly the physicochemical background necessary to understand paramagnetic and diamagnetic contrast enhancement with a special reference to novel Magnetization Transfer and ^{13}C Hiperpolarization strategies. We describe then the main macrocyclic structures used to support the environmentally sensitive paramagnetic sensors, including CEST and PARACEST pH sensitive probes, temperature probes and enzyme activity or gene expression activatable probes. Finally we address the most commonly used diamagnetic contrast agents including imidazolic derivatives to reveal extracellular pH and tissue pO_2 values by MRS. The potential applications of these agents in mutimodal and molecular imaging approaches are discussed.

Key words: Magnetic Resonance Imaging, Magnetic Resonance Spectroscopy, Tissue Microenvironment, Contrast Mechanisms, Paramagnetic Contrast Agents, Diamagnetic Contrast Agents, ^{13}C Hyperpolarized molecules, Molecular Imaging.

1. INTRODUCTION

< Figure 1, near here>

The extracellular space of tissues is located between the cellular architectures and the capillary network providing a vital environment for intercellular communication and regulatory metabolic interactions (Figure 1). The biochemical profile of this compartment modulates many vital intracellular functions including differentiation [1], tissue regeneration [2], angiogenesis [3], metastasis [4], proliferation [5] and apoptosis [6] or necrosis [7], among others. The extracellular "millieu" is characterized by a collection of environmental properties, such as pH, pO_2, ionic composition or diffusion, which are significantly different from those present in the intracellular or vascular spaces, configuring in this way a physiologically distinct compartment (Figure 1). Alterations in the environmental properties are known to occur very early during disease development, providing precious information for the diagnosis, prognosis and therapy assessment of the most prevalent and morbid pathologies in developed countries, with particular emphasis in cancer and ischemic episodes [8-10]. On these grounds, non invasive imaging of the extracellular microenvironment has gained substantial scientific and clinical interest in the last decades [11-13]. The biochemical properties of this compartment result from the balance between the cellular uptake and metabolism of substrates as glucose and oxygen from the capillaries, and the removal of waste products as lactate and H^+ through the tissue microvasculature (Figure 1A). Intracellular oxidative metabolism leads simultaneously to the production of freely diffusing CO_2 and water (in fast equilibrium with HCO_3^- and H^+ through carbonic anhidrase). Reductions in glucose or oxygen delivery either by systemic metabolic limitations or inadequate performance of the local capillary network, result in extracellular lactate and proton accumulation, two conditions commonly found during the early development of

most pathologies (Figure 1B). Environmentally sensitive contrast agents (CA´s) are molecules designed to respond to physiopathological alterations in the values of extracellular pH, pO_2, lactate, glucose, ions as Ca^{2+} or Zn^{2+}, red-ox state or even temperature, in a manner detectable by MRI or MRS methods [14-17]. A variety of paramagnetic and diamagnetic "smart CAs" have been designed for this purpose. This review provides an integrative overview on the development and properties of these agents.

The first generation of CA´s included highly stable paramagnetic lanthanide chelates with linear or macrocyclic ligands derived from diethylendiaminopentaacetic acid or tetraazamacrocyclic structures. These complexes, despite proving considerable capacity to reduce the relaxation times of tissue water in vivo, remained non specific hampering to obtain the microenvironmental information desired from the observed contrast enhancement. Improvements in the understanding of the structural and dynamic determinants of water relaxation in the presence of paramagnetic chelates, allowed for the rational design and synthesis of optimized ligands and chelates with improved relaxivity and fine-tuned sensitivity to microenvironmental factors [16,18-20]. Despite spectacular improvements, the use of environmentally sensitive paramagnetic chelates is, however, not devoid of important drawbacks under in vivo conditions. In particular, the relaxivity effects observed may derive frequently, from factors additional to those being investigated including the concentration of the probe or the environmental effects of microviscosity, limited water diffusion and eventually local temperature changes. These uncertainties prompted the development of alternative diamagnetic probes able to determine the microenvironmental properties in vivo in the absence if these interferences [21].

In parallel with the development of MR imaging strategies, early progress in localized Magnetic Resonance Spectroscopy methods, allowed to obtain the metabolic fingerprint of healthy and diseased tissues and lesions [22]. The initial in vivo spectra localized a single tissue volume, but could soon be resolved in space generating multivoxel ^{1}H and ^{13}C MRSI spectroscopic maps with resolution approaching that provided by Possitron Emission Tomography (PET) and other nuclear medicine techniques [23]. However, as in the case of MRI, the MRS observation of endogenous metabolites did not disclose directly the properties of the extracellular environment. This made it necessary to synthesize novel collections of "ad hoc" exogenous diamagnetic sensors able to reveal, the values of tissue pH and pO_2, not previously obtainable from the profile of endogenous metabolites.

In this work we wish to provide an integrative view on the arsenal of paramagnetic and diamagnetic contrast agents currently available to investigate the tissue microenvironment. We begin by introducing the physicochemical background supporting the paramagnetic and diamagnetic strategies of environmental contrast enhancement. We then describe the paramagnetic ligands and chelates most commonly used in these studies. To finalize, we address the use of environmentally sensitive diamagnetic contrast agents currently available for the MRI/MRS approaches. Many related topics could not be covered here to make this review compatible with the allowed length. In particular, the following literature is recommended to complement and extend the information on synthesis and coordination chemistry of macrocyclic structures [24-27], their coupling to proteins or antibodies for cell targetting [28,29], superpaparamagnetic or ferromagnetic nanoparticles [30,31] or liposome formulations [32-34]. A comprehensive perspective on the fundamentals of paramagnetic relaxation and the early agents may be found the classical books edited by Merbach and Toth [35]

or Krause [36], and in the reviews of refs. [18,37-39]. Earlier accounts on diamagnetic probes may be found in [21]. Finally, for comprehensive information in novel nanotechnology approaches and liposomal formulations the reader is referred to refs. [40-42].

2. AN INTEGRATIVE VIEW ON PARAMAGNETIC AND DIAMAGNETIC CONTRAST

Contrast enhancement in MRI or MRS (Δ_c) may be defined as the difference in intensity between the same pixel or the same collection of pixels (region of interest) in the pre-contrast (I_{pre} or $\bar{I}_{pre}$) and post-contrast (I_{post} or $\bar{I}_{post}$) MR images;

$$\Delta_c = I_{pre} - I_{post} \approx \bar{I}_{pre} - \bar{I}_{post} \quad (1)$$

Enhanced image contrast may be then, produced by any differential manipulation of the I_{post} intensity, normally achieved through the administration of an adequate exogenous contrast agent or probe. Paramagnetic contrast agents increase Δ_c by modifying the relaxation properties of tissue water in the regions where they accumulate, while diamagnetic contrast agents enhance spectroscopic images by introducing new resonances from the exogenous spectroscopic probe. Notably, both approaches are able to induce the same Δ_c becoming entirely comparable from this perspective. However, diamagnetic and paramagnetic contrast agents are normally treated independently in the literature. Here we aim to combine both approaches, since both seek to improve Δ_c. The intracellular, extracellular or vascular confinement of the administered diamagnetic or paramagnetic probe determines the compartmental origin of image contrast observed. Endogenous metabolites are normally considered to have a primarily intracellular

origin, while exogenous paramagnetic and diamagnetic probes are thought to enhance contrast derived from the extracellular and vascular environments.

3. FUNDAMENTALS OF PARAMAGNETIC CONTRAST ENHANCEMENT

The ability of paramagnetic probes to increase the relaxation rates $r'_{1,2,2*}$ of solvent water is a linear function of the concentration of the contrast agent [CA], the slope of which is known as $r_{1,2,2*}$ relaxivity (measured in $s^{-1}.mM^{-1}$);

$$r'_{1,2,2*} = r^0_{1,2,2*} + r_{1,2,2*}[CA] \quad (2)$$

where $r^0_{1,2,2*}$ represent the relaxation rate of the water protons in the absence of contrast agent [43]. The higher the relaxivity of the probe the more potent and sensitive the agent becomes and the smaller the concentration required to obtain MRI detectable changes in water relaxation [18].

< Figure 2, near here>

The enhancement in the water relaxation rate originates from the direct contact of one or more water molecules with the unpaired electron(s) of the paramagnetic metal. Paramagnetic contact results in a transfer of electronic magnetization that reduces relelaxation times of the coordinated water molecule (T_{1m}), which then exchanges fast with the remaining water molecules of the solvent (k_{ex}), magnifying enormously the effects of the initial paramagnetic interaction. Gd(III) was chosen as the optimal paramagnetic lanthanide because of its seven unpaired electrons in d orbitals (the largest within the lanthanide series) and its relatively slow electronic relaxation rate (ca. 10ps). Both circumstances provide the most intense paramagnetic effect among the lanthanide series and the longest electronic magnetization transfer period during the residence time of the coordinated water molecule over the paramagnetic ion. However, free Gd(III) ions are toxic in vivo, mostly because of their very favourable competition with the

endogenous Ca^{2+} ions necessary for the operation of many biochemical and physiological processes. This circumstance imposed, for safety reasons, to use Gd(III) chelates with extremely high kinetic and thermodynamic stability, rather than the free, hydrated Gd(III) ion [44]. Upon chelation, up to eight sites out of the nine available in Gd(III) are occupied by the polydentate ligand, leaving normally only one vacant site for water contact and exchange. Even with this precaution, the possibility of transmetallation in vivo is not negligible. The competitive substitution of chelated Gd(III) by physiologically competing metals (Ca^{2+}, Zn^{2+} or Mn^{2+} among others), liberating free Gd(III) into the tissue entails considerable risk, probably underlying some of the nephrogenic cystic fibrosis cases observed in renally compromised patients after repeated administration of some Gd(III) chelates [45-47]. In addition to Gd(III) many other paramagnetic metals may be used (although less efficiently) for these purposes, including mainly Dy(III), Eu(III), Mn (II) or Fe(III).

The relaxation enhancement induced in water by paramagnetic ions involves two different effects; the inner (r_{is}) and outer (r_{os}) sphere contributions to relaxivity, each one representing approximatelly 50% of the total relaxivity observed [18,37,43,48]. Inner sphere contributions are due to those water molecules in direct contact with Gd(III) ion, while outer sphere effects involve the contributions of solvent molecules external to the complex, but still maintaining an efficient exchange with those of the inner sphere. Only the inner sphere effects can be adequately modulated by manipulating the chemical structure of the ligand. Very briefly, the relaxation of water molecules in the inner sphere of a paramagnetic chelate may be described theoretically by an intricate, highly non linear function of the number of water molecules coordinated to the paramagnetic metal (q), the correlation time of the complex (τ_c) and the exchange

rate (k_{ex}) of water molecules in the inner coordination sphere of the paramagnetic metal [18,37,43,48];

$$r_{1is} = f(q, \tau_c, k_{ex}) \quad (3)$$

The first improvements in the structure of the ligands agents seeked to improve their relaxivity values. Relaxivity of the early chelates lied in the range 3-4 $s^{-1}.mM^{-1}$, being significantly smaller value than the predicted theoretical limit of ca. 100 $s^{-1}.mM^{-1}$. Increasing the q values, slowing down the molecular rotation τ_c (e.g. by increasing the molecular weight of the complexes using dendrimeric materials or binding to macromolecules) and favouring a faster water exchange (increased k_{ex}), produced significant increases in relaxivity reaching the 30-40 s^{-1} mM^{-1} range. This knowledge on the determinants of relaxivity and their structural basis allowed then for the design of activatable probes, showing relaxivity changes in response to environmental factors as temperature, pH, metabolites, enzymatic activity or even gene expression through the effects of these variables of q, τ_c or k_{ex}, respectively [14,16].

4. FUNDAMENTALS OF DIAMAGNETIC CONTRAST ENHANCEMENT

In addition to the paramagnetic probes, contrast in Magnetic Resonance Images may be improved by diamagnetic methods through the selective perturbation of the chemical exchange of endogenous water molecules or the selective enhancements of their different diffusional components. Spectroscopic methods add to these classical diamagnetic imaging approaches by providing spectroscopic probes sensitive to microenvironmental factors as pH or pO_2. While it is possible to discriminate between the intra- and extracellular environment because of the faster water diffusion in the later, perturbations involving water exchange are more difficult to interpret, since magnetically labelled water may exchange between the intra- and extracellular

environments several times during the measurement time, providing a weighted average of the contribution from these two environments. In spite of this, it is normally convened in all these cases, that the use of non permeable exogenous probes primarily reflects the properties of vascular and extracellular compartments while the use of endogenous metabolites reflect mainly the intracellular environment.

Chemical Exchange

<Figure 3, near here>

The most abundant endogenous diamagnetic probe in vivo is the water molecule, accounting for approximately 80% of the tissue weight in adult mammals [49]. The presence of at least two dynamically different and mutually exchanging types of water molecules in vivo, those freely mobile and those trapped as solvation water in biomacromolecules, open the possibility to enhance contrast by manipulating this exchange [50]. The method is based in the early proposal of Forsen and Hoffman to determine exchange rates through saturation transfer experiments [51]. Free solvent water has a fast rotational and translational correlation time ca. 1 ps originating a narrow resonance, while solvation water, partially immobilized over the surface of macromolecules, acquires the macromolecular rotational and translational dynamics (in the ns range) originating a downfield shifted (typically 2-4 ppm), broad, water resonance [49]. This dynamic difference underlies an interesting source of MRI contrast based in the exchange between these dynamically different environments (Chemical Exchange Saturation Transfer, CEST) [52]. First, for this two populations of water molecules to be resolved as two resonances, the exchange rate k_{ex} between them must be slower than the chemical shift difference $\Delta\omega$ between both resonances ($\Delta\omega >> k_{ex}$). Under these conditions, it is possible to saturate the broad component and observe a decrease in the intensity of the narrow one. The faster the exchange k_{ex} between these

populations, the more saturation transfer is observed [53]. However, the exchange rate can never exceed the "slow exchange" limit ($\Delta\omega >> k_{ex}$), so the approach is inherently limited to measure rates slower than $\Delta\omega$, normally few ^{1}H NMR ppm between diamagnetic molecules (DIACEST). Notably, it is possible to increase dramatically $\Delta\omega$ by using lanthanide "shift reagents". These molecules are chelates of different lanthanides, particularly Eu(III) or Dy(III), able to increase $\Delta\omega$ up to ca. 50 ppm, improving considerably the range of exchange rates measurable. Moreover, different $\Delta\omega$ can be induced using different lanthanides, an opportunity that allows to "fine tune" different saturation frequencies for different purposes, through the use different lanthanide complexes, even if the same ligand is used.

The saturation transfer phenomenon is not restricted to exchanges between water molecules. In the Amide Proton Transfer (APT) method, the exchange of magnetization between the amide protons from tissue peptides and proteins and those of solvent water is observed [54]. In these cases it is possible to induce decreases in the solvent water resonance intensity after irradiating the amide region, the effect being larger for larger protein concentrations, a circumstance that allows the estimation of protein and peptide concentrations in vivo [55,56].

The exchange of protons between water and the amide protons is pH dependent, allowing also the investigation of tissue pH from the exchange rates determined by Chemical Exchange Saturation Transfer with a variety of diamagnetic molecules including proteins [57-59]. The compartmental origin of the dominant exchange mechanism determines the physiological environment where the pH is monitored. In the APT method, the pH value visualized corresponds most probably to the intracellular compartment, since the intracellular protein and peptide concentrations are larger than those in the extracellular space. This approach may be also enhanced to the use of

exogenous pH sensitive paramagnetic chelates (PARACEST) [14,16]. In these cases the exchange of water molecules between the coordination sphere of the paramagnetic center and the bulk solvent is also pH sensitive. Since these probes are mainly extracellular, the pH values visualized are thought to correspond primarily to the extracellular environment. PARACEST approaches entail enormous versatility since different environmental properties may visualized in the same imaging experiment by using selective irradiation frequencies of a suitable collection of lanthanide chelates with different $\Delta\omega$. In should be possible then to obtain intra- and extracellular pH images from the same tissue using endogenous and exogenous CEST and PARACEST agents.

Translational diffusion

< Figure 4, near here>

The translational movements of water provide an additional opportunity to induce and observe tissue contrast since they can be conveniently monitored by diffusion weighted MRI methods [60]. Following the Stokes-Einstein relationship, the Apparent translational Diffusion Coefficient (ADC) of water is highly dependent on the molecular obstructions that the water molecule finds in its random movements. These obstructions are higher in the intra- than in the extracellular environments, resulting in slower intracellular diffusion. Moreover, it has become recently possible to explore the translational diffusion of water in any direction of space, simply by modifying the orientation of the applied diffusion sensitizing gradient [61]. This made it possible to unravel the dominant direction of translational water movements solving the diffusion tensor, a procedure allowing, in the central nervous system, the detection of the faster diffusion of water molecules through the neuronal axons and the preparation of maps of neuronal tracts through the white matter [62]. To our knowledge, Single Wall Carbon

Nanotubes are the first agent communicated to induce differential diffusion of the water molecules with a predominant direction oriented through the longitudinal axis of the nanotube, allowing in this way to induce exogenous contrast in Diffusion Tensor Images [63].

Spectroscopic methods

pH sensors

The potential to determine pH from MRS measurements was soon realized [64-66]. Briefly, it is possible to measure pH from the changes in chemical shift of a proton (or other magnetically active nucleus) located in or close to an ionisable group in a molecule. In a general reaction of the type

$$A^- + H^+ \rightarrow AH$$

where A- and AH represent the anionic and acidic forms, characterized by chemical shifts δ_{A-} and $\delta_{AH,}$ pH may be calculated from the expression,

$$pH = pK_a + \log ((\delta-\delta_A)/(\delta_{AH}-\delta)) \qquad (4)$$

where pK_a represents the pK_a of the ionisable group in A and δ the observed chemical shift of the pH sensitive proton. The most useful probes in vivo, are those with pK_a values in the vicinity of physiological pH, in the 6.5-7.5 range. The larger the chemical shift interval between δ_A y δ_{AH}, the better the pH resolution from the δ measurement. The intra- or extracellular location of the pH probe allows for the measurement of either intra- or extracellular pH. Inorganic phosphate and phosphonate derivatives, have been classically used as intra- or extracellular probes in ^{31}P NMR [67,68], while non permeant imidazolic derivatives were implemented more recently to measure extracellular pH with the inherently increased sensitivity and spatial resolution provided by ^{1}H NMR [69]. The imidazolic H2 proton, reflecting the ionization state of the N3 nitrogen, is normally used for these purposes since; (i) it is conveniently located in the

aromatic region and thus, not interfering with the endogenous metabolite resonances and (ii) depicts a relatively large chemical shift variation of ca. 1ppm in the physiological pH range [70].

pO_2 sensors

< Figure 5, near here>

Nitroimidazoles have been classically used as probes to detect hypoxia in a variety of imaging modalities including MRI (^{19}F and ^{1}H), PET (Figure 8b),[71,72] SPECT [73] and optical methods (Figure 8c)[74,75].

Briefly, the nitro group depicts a redox potential similar to NAD(P)H and is reduced in vivo under hypoxic conditions to very unstable hydroxylamine or amine derivatives that react easily with intracellular electrophiles to form adducts [76]. The chemical reduction of hydroxylamine derivatives and the subsequent chemical transformations have also been investigated [77,78], however the precise mechanism of nitroimidazole reduction in vivo remains still incompletely understood.

Several attempts have been made to design rationally an optimized oxygen sensor based on nitroimidazole derivatives. The structure of most nitroimidazole based sensors (Figure 5a) may be divided in two parts: the nitro moiety and the lateral chain. The former is linked to an aromatic ring (usually imidazole) and is responsible of bioreduction of the molecule. The lateral chain is responsible of biodistribution, tissue penetration, elimination rate, etc.[79], carrying in most cases the “chromophore atoms” (^{19}F, ^{18}F, $^{125/123}$I, ^{99m}Tc). The general properties of these molecules may be, thus, fine tuned for specific purposes by modifying appropriately either the imidazol ring or the lateral chain, respectively. The improvements achieved may include: enough solubility in aqueous medium balanced with and adequate lipophilicity, stability and more feasible syntheses.

Hyperpolarized sensors

Spectacular increases in ^{13}C NMR sensitivity of up to 10.000 times have been obtained by hyperpolarizing ^{13}C enriched substrates opening an avenue to ^{13}C imaging of endogenous metabolites in health and disease [80-82]. Several hyperpolarization strategies have been described including the Brut Force method, the Optical Pumping method, the Parahydrogen method and the Dynamic Nuclear Polarization (DNP) method [83,84]. Of these the most relevant for environmental purposes is the DNP method. The technique is based in the transfer of electronic magnetization from a Gd(III) to the ^{13}C nucleous, in the solid state and at very low temperature (4K), with the help of a suitable catalyst. The hyperpolarized ^{13}C molecule can then be transferred into solution [85], injected in animals or administered to cells, and its metabolism followed kinetically by ^{13}C NMR and resolved in space by ^{13}C MRSI [86], for a period as long as the hyperopolarized state lasts, normally less than 200 s. Endogenous HCO_3^- is normally observed after the administration of (1-^{13}C) pyruvate or (1-^{13}C) lactate, after decarboxilation by pyruvate dehydrogenase in the tricarboxylic acid cycle [87,88]. The carbonic anhydrase equilibrium (Eq. 5) is sensitive to pH, making it possible to determine pH from the relative intensities of the resonances of $^{13}CO_2$ and $^{13}CO_3H^-$ resonances [89,90];.

$$CO_2 + H_2O \quad \leftrightarrow \quad CO_3H^- + H^+ \qquad (5)$$

4. PARAMEGNETIC AGENTS

pH sensors

Relaxivity probes

<Figure 6, near here>

Complexes showing pH dependent relaxivity are of particular interest since they may afford to distinguish rather easily, cancerous or ischemic tissues (pH_e = 6.6-6.9) from the surrounding healthy tissue (pH_e = 7.2). In these cases, the protonation of a donor atom (O or N) in the complex may change the conformation of the pending arms and allow for competitive binding of an additional water molecule, increasing in this way the q value and the relaxivity of the complex. The first generation of paramagnetic complexes revealing pH changes consisted of Gd(III)DOTA derivatives containing amide or phosphonate pending arms [91,92]. $Gd(DOTAM\text{-}MP)^{3+}$ (Figure 6A) [92] shows several pH jumps in its relaxivity between pH 3 and 8. NMR studies indicate that Ln(III) ion is bound by the four amide O-atoms and the four N-atoms of the cyclen backbone and that the first coordination sphere is completed by a water molecule. The phosphonate groups are not coordinated to the Ln(III) ion and are responsible of the pH dependence. This is so because the pK_a of phosphonates is in the physiological range, making these agents to show pH dependent relaxivity, through the opening or closing of the phosphonate structure. This circumstance facilitated or hampered water contact with the Gd(III) core and thus sensitized to pH the relaxivity value. Calibration of the dependence of relaxivity with pH allowed the determination of pH from relaxivity measurements. An important limitation of the method was, however, that relaxivity of the CA was dependent also on the CA concentration, making it difficult to discriminate in vivo if the observed change in relaxivity was derived from a change in pH or a change in the concentration of the probe. In spite of this, valuable measurements of extracellular pH were performed after dual administration of pH responsive and non responsive agents [93-95] or through the application of T_1/T_2 ratiometric methods [96].

In a different approach (Figure 6B), the binding of water molecules to the paramagnetic center under ambient conditions is prevented by the interaction of

hydrogen carbonate with the metal ion in a macrocyclic tetraazatriamide complex, Gd(DO3A-Ala) [91,97]. In an acidic medium (pH < 6), the hydrogen carbonate ion will be protonated and displaced by two water molecules resulting in an increase of the complex relaxivity. Finally, metabolites other than protons and water may be imaged using the important effects on the relaxivity of Gd(III) DO3A induced by lactate or inorganic phosphate, provided the effects of agent concentration can be corrected [98].

PARACEST probes

The use of the pH dependence of the rate constant for Chemical Exchange between water and an ionizable group of the agent has been used recently to measure pH and other environmental factors by Magnetization Transfer methods [16,99-101]. This approach overcomes one of the most important limitations of the relaxivity method, making the measurement independent of the concentration of the agent utilized. Upon saturation of the exchangeable resonance, a decrease is observed in the intensity of the free water resonance that is proportional to the rate constant of exchange between both sites, and thus to pH. The initial pH sensitive diamagnetic agents (DIACEST), as barbituric acid, required large concentrations (ca 60 mM) for an appreciable effect on the MR image [58,59] although protocols to decrease the large concentrations required have been proposed more recently [102]. An interesting variant of this method used endogenous polypeptides, whose large number of pH sensitive, water exchanging, amide bonds (Amide Proton Transfer, APT) decreased drastically the polypeptide concentration necessary to observe the magnetization transfer (MT) effect [53,55,57]. As mentioned above, an important limitation of the pH measurement by DIACEST methods is the restricted dynamic range of rate constants obtainable, derived from the "slow exchange" limitation between resonances separated only by ca. 3 ppm.

DIACEST molecules were soon followed by the PARACEST probes, comprising basically complexes with different lanthanides and ionizable groups, depicting enormous "paramagnetic shifs" $\Delta\omega$ (ca. -50 ppm), exchanging magnetization with the surrounding water in a pH dependent manner (Figure 6C) [16,103]. Weakly paramagnetic complexes from amide cyclen derivatives have shown to act as suitable MT contrast agents (Figure 6C). The Eu(III) complex from ligand **1** has a bound-water resonance near δ = 50 ppm, with an exchange lifetime of approximately 350 μs, acting as a powerful PARACEST agent [100]. The corresponding complexes of **3** with lighter Ln(III) ions (Pr, Nd, and Eu) are also pH responsive "single-molecule CEST agents" [100]. The Yb(III) complex from **1** with eight exchangeable, hyperfine-shifted amide protons, is reported as a prototype of high-sensitivity MT agent [92] .

Eu(III) complexes of cyclen-based ligands have been proposed additionally as glucose and lactate sensors by CEST imaging detection [100,104,105]. Both, the free ligands and their Eu(III) complexes bind selectively simple sugars, with different binding affinities depending on the sugar structure. Recently, nitric oxide has been added to the molecules potentially detectable by CEST agents [106]. Finally, a variety of PARACEST probes have been proposed to detect in vivo temperature [107,108].

The CEST and APT methods, although brilliantly performing in vitro, present also some difficulties of interpretation in vivo. In particular, the intra- or extracellular origin of the MR effect (or pH measurement) is difficult to establish, since the magnetized water molecule that exchanges with the probes may move in and out of the cell during the imaging time, resulting in an averaged contribution of these two different environments to the pH value determined. In addition, the possibility that additional magnetization exchanges occur between water molecule and other endogenous ionizable groups from the tissue, cannot be completely excluded, probably masking in

part an accurate pH measurement. Finally, since pH dependent exchange is a diffusion limited process, local changes in the apparent diffusion coefficient of water could contribute as well to the pH measurement, introducing additional sources of uncertainty on the accuracy of the pH value measured in vivo using this method.

Other probes

In addition to pH, the cyclen structure may be sensitized to a variety of additional circumstances including Ca^{2+}, enzyme activity, gene expression, temperature, lactate or glucose, providing the most versatile platform currently available for environmental studies. Interestingly, Meade and co-workers reported a calcium sensitive contrast agent, Gd_2(DOPTA) [45]. The ligand consists of two DO3A units that are linked via an EGTA [29] type spacer carrying two aromatic iminodiacetate groups. In the absence of Ca^{2+}, the iminoacetate functions are coordinated to the Gd(III) ions which under these conditions are inaccessible to water. However, in the presence of Ca^{2+}, the carboxylate groups rearrange to bind this ion and two vacant coordination sites on each of the Gd(III) ions are now able to bind water molecules. This results in an increase in the relaxivity from 3.26 to 5.76 s^{-1} mM^{-1}.

MR images from healthy and diseased tissues would greatly benefit from the detection of gene expression in vivo [109,110]. The first contrast agent reporting enzyme activity described in the literature was Gd(DO3A-gal), a DOTA type ligand in which one of the carboxylate groups is replaced by a galactose moiety [46,[111]. The galactose moiety protects the metal ion from water binding. As soon as the enzyme β-galactosidase cleaves off the sugar, $[Gd(DOTA)]^-$ is formed with the inner sphere accessible for the coordination of a water molecule, with the consequent increase in relaxivity. Since many exogenously administered genes carry the flanking β-galactosidase gene, expression of these transgenes may be monitored by monitoring in

this way the expression of the β-galactosidase enzyme in vivo. Additional approaches have been proposed for the expression of iron binding proteins or transporters able to be activated by endogenous iron accumulation [112,113] as well as novel gene expression amplification strategies to improve MRI visualization of the overexpressed genes [114].

4. DIAMAGNETIC AGENTS

Imidazole derivatives

Spectroscopic pH responsive probes

< Figure 7, near here>

To overcome some of the limitations of paramagnetic probes, we proposed some years ago the development of a novel series of diamagnetic agents to determine extracellular pH using the alternative Magnetic Resonance Spectroscopy approach [20,21]. 3-(Ethoxycarbonyl)-2-imidazol-1-ylpropionic acid, abbreviated as IEPA (Figure 7), was the first probe synthesized in our laboratories already in 1992, that made possible the non-invasive in vivo measurement of pH_e in tumours using of the ^{1}H-NMR Spectroscopic Imaging (^{1}H MRSI) method [22]. We selected the imidazole ring in the design of IEPA basically for two reasons: i) the imidazole pK_a (ca. 7.0) is very close to physiological pH allowing accurate pH measurements, and ii) its H-2, H-4 and H-5 proton resonances are easily resolved and observed in the aromatic region of ^{1}H NMR spectra, sufficiently far away from the water and the crowded aliphatic regions of the spectrum.

< Figure 8, near here>

Figure 8 illustrates the method with one the earliest pH images obtained. After infusing IEPA in rat bearing a C6 glioma, it was possible to observe the resonances from the H2 proton of the pH probe, only in the tumoral region [115,116]. This is

because IEPA is a non permeant probe and the tumor vasculature is devoid of blood brain barrier, allowing IEPA to diffuse directly into the extracellular space. Calibration of the pH dependence of the H2 chemical shift, allowed then to determine extracellular pH. H2 Multiple, localized, pH_e measurements using this probe were conveniently obtained by determining the chemical shifts of its imidazolic H-2 proton in the collection of contiguous voxels provided by the ^{1}H MRSI experiment. It was possible then to demonstrate for the first time that extracellular pH is heterogenous through the tumor (Figure 8f).

The same ^{1}H MRSI approach, with a longer echo time (120 ms), could be used to obtain maps of other endogenous metabolites of the C6 glioma, allowing for the first time to establish correlations between extracellular pH and the local concentrations of the different metabolites imaged. The correlation found between the lactate resonance and the extracellular pH in vivo entailed particular physiological relevance. The classical work of Warburg had revealed that tumors produced larger amounts of lactate than normal tissues, indicating that extracellular lactate could be the main cause of extracellular tumor acidity. Our results in vivo, revealed no significant correlation between extracellular pH and the lactate resonance, indicating that either protons diffuse faster than lactate from the lactate production sites or, that tumors present additional sources of protons to lactate. We confirmed recently this observation using ISUCA, an improved pH indicator based on the IEPA structure but providing increased blood retention time and augmented pH resolution [116]. In summary, the use of diamagnetic pH probes and in vivo MRSI provides a good illustration of the important differences between metabolism as investigated in isolated cells or tissues or in vivo, illustrating the enormous potential of accurate pH measurements by ^{1}H MRSI as a new diagnostic and prognostic tool in oncology.

Spectroscopic pO_2 responsive probes

Varghese *et al.* reported firstly, to our knowledge, that -^{14}C labeled-misonidazole was selectively trapped in oxygen deficient cells [117]. Various attempts have been reported using nitroimidazole based drugs as ^{19}F-NMR oximetry probes. Early work carried out by Raleigh *et al.* using CCI-103F showed the *ex vivo* detectability of bounded derivatives in tumour and liver by ^{19}F-NMR [118]. Later on, the *ex vivo* the concentration of bound marker in different types of subcutaneous tumour (R3327 H or R3327 AT prostatic adenocarcinomas and walker 256 carcinoma) and in liver was quantified using ^{19}F-NMR [119].

More recently, two fluorinated nitroimidazole derivatives, SR-4554 and TF-MISO (Figure 5A) have been used to measure hypoxia *in vivo*. The former has been extensively studied both *in vitro* [120] and *in vivo* with different tumour types [121] showing low toxicity, high metabolic stability, favourable pharmacokinetics and high sensitivity for detection by magnetic resonance spectroscopy[122]. A close relationship between retention of SR-4554 and polarographic pO_2 electrode measurements in rat bearing P22 carcinosarcoma has been reported [123]. SR-4554 has recently entered in Phase I clinical trials showing promising pharmacokinetic and toxicity profiles, although no oxygenation measurements have been reported to date, to our knowledge, in patients [124].

TF-MISO has been proposed as a plausible ^{19}F-NMR nitroimidazole based reporter [125]. A positive correlation is found *in vivo* between the corresponding retention index and the tumour volume (qualitatively related with tumour hypoxia). It is important to notice that multivoxel spectroscopy has been achieved in tumours *in vivo*, showing that TF-MISO is visible under these conditions. Based on spectroscopy measurements, tumor hypoxic fraction was calculated, finding similar results with

literature values for MCa tumors. Although this methodology remains still far from being clinically applicable, it represents an important advance since it proves for the first time that a nitroimidazole based drug may be spatially resolved by multivoxel spectroscopy *in vivo*.

Hyperpolarized probes

<Figure 9, near here>

The use of hyperpolarized ^{13}C methods and $^{13}CO_3H$- to measure metabolic fluxes and pH in vivo is well illustrated recently in the studies from the Cambridge, Oxford and Dallas groups [89,126-129]. The method allows to measure pH from the ratio of $^{13}CO_2/CO_3H^-$ resonances, maintained in, or near equilibrium, by carbonic anhidrase. Figure 9 illustrates the pH results obtained in vivo in an implanted lymphoma after the administration of hyperpolarized (1-^{13}C) pyruvate using ^{13}C MRSI. The resolution is comparable to that obtained by ^{1}H MRSI, but its applicability remains at present limited to few research sites because the large and specialized infrastructure required. An important concern in this case may arise from the characterization of intra- or extracellular environments originating the observed $^{13}CO_2$ or HCO_3^- resonances, because the ubiquitous location of these two metabolites in vivo. However, it appears reasonable to believe that value of pH measured by hyperpolarized techniques refers primarily to the intracellular compartment, since it correlates well in the heart with ^{31}P NMR measurements of pH_i using the inorganic phosphate measurement.

5. CONCLUDING REMARKS AND FUTURE PERSPECTIVES

The present review addressed briefly the use of MRI or MRS probes to obtain measurements of microenvironmental variables as pH and pO_2 in vivo. MRI active contrast agents provide values of these variables with high spatial resolution. However,

the possibility that MRI measurements include contributions from environmental factors additional to those being investigated, such as transcellular water exchange or limited diffusion between intra- and extracellular spaces, should not be ignored. In contrast, diamagnetic probes for spectroscopic imaging provide measurements of extracellular pH with lower resolution, but entailed with a more robust, unambiguous interpretation. The recent improvements of the available agents using magnetically equivalent dimer molecules [26], together with the rapidly increasing magnetic fields available for spectroscopy promise to improve in the near future the resolution of the MRSI experiments approaching the MR imaging limits.

In virtually all previous cases, paramagnetic or diamagnetic agents have been used in separate. Necessary cross-validations of the measurements need them to be applied in combination in the same experimental model. Moreover, the combination of the optimized pH_e diamagnetic probes with recently synthesized pO_2 probes [27], and PARACEST probes sensitive to glucose or lactate concentrations may afford, in the near future, for the integral evaluation of the various environmental factors in normal and diseased tissues by MRI/MRS methods. The spectacular improvements in the use of ^{13}C hyperpolarized probes promise to unravel the relationships between pH and pO_2 measurements and the activity of crucial enzymes of energy metabolism as pyruvate dehydrogenase or lactate dehyrogenase. It is also possible to think that some the diamagnetic probes currently available may become ^{13}C enriched and hyperopolarized in the future, further enlarging the arsenal of hyperpolarized environmental probes. Finally, the Blood Brain Barrier remains as one of the most important challenges to allow these probes to reach and investigate the extracellular environment of the healthy brain in vivo. Structural improvements are expected to increase significantly the pass of

environmentally sensitive probes through the barrier into the extracellular compartment of the healthy or diseased brain.

In summary, the present review has shown that imaging the tissue microenvironment in vivo is feasible and has demonstrated great potential in animal models of disease, its transfer to the clinic remaining at present the most important challenge for future developments in this field.

ACKNOWELEDGEMENTS

This work was supported in part by grants: CTQ2006-06505/BQU, CTQ2009-14146-C01/C02, to P.B. and P.L.L., S-BIO/0179/2006 and SAF2008/01381 to SC and EU MEDITRANS Integrated Project NMP4-CT-2006-02668 to S.C., P.L.L. and P.B. J. P-T, D. C., B.L. and V.N. are predoctoral fellows from the Community of Madrid and CSIC and V.N. and C.U hold contracts from UNED. Authors are indebted to Mr. Javier Pérez for carefully drafting the illustrations.

ABBREVIATIONS

T_1 : Longitudinal Relaxation time

T_2 : Transversal relaxation time

T_{2*} : Transversal relaxation time including magnetic field inhomogeneity

r_1 : Longitudinal relaxation rate

r_2 : Transversal relaxation rate

r_{2*} : Transversal relaxation rate including magnetic field homogeneity effects

ADC : Apparent Diffusion Coefiicient

MT : Magnetization Transfer

MRSI: Magnetic Resonance Spectroscopic Imaging

CEST: Chemical Exchange Saturation Transfer

DIACEST: Diamagnetically Induced Chemical Exchange Saturation Transfer

PARACEST: Paramagnetically Induced Chemical Exchange Saturation Transfer

APT: Amide Proton Transfer

DTPA: Diethylen diamino pentaacetic acid

DNP: Dynamic Nuclear Polarization

REFERENCES

[1] Elaut, G.; Henkens, T.; Papeleu, P.; Snykers, S.; Vinken, M.; Vanhaecke, T.; Rogiers, V. Molecular mechanisms underlying the dedifferentiation process of isolated hepatocytes and their cultures. *Curr. Drug Metab.* **2006,** *7*, 629-60.

[2] Xiang, S.; Pan, W.; Kastin, A. J. Strategies to create a regenerating environment for the injured spinal cord. *Curr. Pharm. Biotechnol.* **2005,** *11*, 1267-77.

[3] Munoz-Chapuli, R.; Quesada, A. R.; Angel Medina, M. Angiogenesis and signal transduction in endothelial cells. *Cell. Mol. Life Sci.* **2004,** *61*, 2224-43.

[4] Cairns, R. A.; Khokha, R.; Hill, R. P. Molecular mechanisms of tumor invasion and metastasis: an integrated view. *Curr. Mol. Med.* **2003,** *3*, 659-71.

[5] Pathania, M.; Yan, L. D.; Bordey, A. A symphony of signals conducts early and late stages of adult neurogenesis. *Neuropharmacology*.

[6] Haddad, J. J. Oxygen-sensing mechanisms and the regulation of redox-responsive transcription factors in development and pathophysiology. *Respir. Res.* **2002,** *3*, 26.

[7] Taoufik, E.; Probert, L. Ischemic neuronal damage. *Curr. Pharm. Biotechnol.* **2008,** *14*, 3565-73.

[8] Gatenby, R. A.; Gillies, R. J. A microenvironmental model of carcinogenesis. *Nat. Rev. Cancer* **2008,** *8*, 56-61.

[9] Joyce, J. A.; Pollard, J. W. Microenvironmental regulation of metastasis. *Nat. Rev. Cancer* **2009,** *9*, 239-52.

[10] Meads, M. B.; Gatenby, R. A.; Dalton, W. S. Environment-mediated drug resistance: a major contributor to minimal residual disease. *Nat. Rev. Cancer* **2009,** *9*, 665-74.

[11] Sloane, B. F.; Gillies, R. J.; Mohla, S.; Sogn, J. A.; Menkens, A. E.; Sullivan, D. C. I2 imaging: cancer biology and the tumor microenvironment. *Cancer Res.* **2006,** *66*, 11097-9.

[12] Jordan, B. F.; Runquist, M.; Raghunand, N.; Baker, A.; Williams, R.; Kirkpatrick, L.; Powis, G.; Gillies, R. J. Dynamic contrast-enhanced and diffusion MRI show rapid and dramatic changes in tumor microenvironment in response to inhibition of HIF-1alpha using PX-478. *Neoplasia* **2005,** *7*, 475-85.

[13] Gillies, R. J.; Raghunand, N.; Karczmar, G. S.; Bhujwalla, Z. M. MRI of the tumor microenvironment. *J. Magn. Reson. Imaging* **2002,** *16*, 430-50.

[14] De Leon-Rodriguez, L. M.; Lubag, A. J.; Malloy, C. R.; Martinez, G. V.; Gillies, R. J.; Sherry, A. D. Responsive MRI agents for sensing metabolism in vivo. *Acc. Chem. Res.* **2009,** *42*, 948-57.

[15] Aime, S.; Castelli, D. D.; Crich, S. G.; Gianolio, E.; Terreno, E. Pushing the sensitivity envelope of lanthanide-based magnetic resonance imaging (MRI) contrast agents for molecular imaging applications. *Acc. Chem. Res.* **2009,** *42*, 822-31.

[16] Sherry, A. D.; Woods, M. Chemical exchange saturation transfer contrast agents for magnetic resonance imaging. *Annu. Rev. Biomed. Eng.* **2008,** *10*, 391-411.

[17] Raghunand, N.; Jagadish, B.; Trouard, T. P.; Galons, J. P.; Gillies, R. J.; Mash, E. A. Redox-sensitive contrast agents for MRI based on reversible binding of thiols to serum albumin. *Magn. Reson. Med.* **2006,** *55*, 1272-80.

[18] Caravan, P. Strategies for increasing the sensitivity of gadolinium based MRI contrast agents. *Chem. Soc. Rev.* **2006,** *35*, 512-23.

[19] Ronald, J. A.; Chen, J. W.; Chen, Y.; Hamilton, A. M.; Rodriguez, E.; Reynolds, F.; Hegele, R. A.; Rogers, K. A.; Querol, M.; Bogdanov, A.; Weissleder, R.; Rutt, B. K. Enzyme-sensitive magnetic resonance imaging targeting myeloperoxidase identifies active inflammation in experimental rabbit atherosclerotic plaques. *Circulation* **2009,** *120*, 592-9.

[20] Querol, M.; Bogdanov, A., Jr. Environment-sensitive and enzyme-sensitive MR contrast agents. *Handb. Exp. Pharmacol.* **2008**, 37-57.

[21] Perez-Mayoral, E.; Negri, V.; Soler-Padros, J.; Cerdan, S.; Ballesteros, P. Chemistry of paramagnetic and diamagnetic contrast agents for Magnetic Resonance Imaging and Spectroscopy pH responsive contrast agents. *Eur. J. Radiol.* **2008,** *67*, 453-8.

[22] Gillies, R. J. Nuclear magnetic resonance and its applications to physiological problems. *Annu Rev Physiol* **1992,** *54*, 733-48.

[23] Skoch, A.; Jiru, F.; Bunke, J. Spectroscopic imaging: basic principles. *Eur. J. Radiol.* **2008,** *67*, 230-9.

[24] Constable, E. C. *Coordination Chemistry of Macrocycles Compounds*. Oxford University Press: New York, 1999.

[25] Pérez-Mayoral, E.; Soler-Padrós, J.; Negri, V.; Cerdán, S.; Ballesteros, P. Synthetic Approaches to Heterocyclic Ligands for Gd-Based MRI Contrast Agents. *Molecules* **2007,** *12*, 1771-1795.

[26] Ballesteros, P. Flexible tetraazamacrocyles as contrast agents for Magnetic Resonance Imaging. In *Research Signpost*, XXX, Ed. 2005; Vol. 1, pp 512-32.

[27] Vincent, J.; Desreux, J.-F. Synthesis of MRI contrast agents II: Macrocyclic ligands. In *The Chemistry of Contrast Agents in Medical Magnetic Resonance Imaging*, Merbach, A. E. a. T., E., Ed. John Wiley and Sons: Chichester, 2002; pp 157-192.

[28] Morawski, A. M.; Lanza, G. A.; Wickline, S. A. Targeted contrast agents for magnetic resonance imaging and ultrasound. *Curr. Opin. Biotechnol.* **2005,** *16*, 89-92.

[29] Aime, S.; Botta, M.; Fasano, M.; Terreno, E. Protein-Bound Metal Chelates In *The chemistry of Contrast Agents for Medical Magnetic Resonance Imaging*, Merbach, A. E. a. T., E., Ed. John Wiley and Sons: Chichester, 2002.

[30] Laurent, S.; Boutry, S.; Mahieu, I.; Vander Elst, L.; Muller, R. N. Iron oxide based MR contrast agents: from chemistry to cell labeling. *Curr. Med. Chem.* **2009,** *16*, 4712-27.

[31] Petri-Fink, A.; Hofmann, H. Superparamagnetic iron oxide nanoparticles (SPIONs): from synthesis to in vivo studies--a summary of the synthesis, characterization, in vitro, and in vivo investigations of SPIONs with particular focus on surface and colloidal properties. *IEEE Trans. Nanobiosci.* **2007,** *6*, 289-97.

[32] Aime, S.; Castelli, D. D.; Crich, S. G.; Gianolio, E.; Terreno, E. Pushing the sensitivity envelope of lanthanide-based magnetic resonance imaging (MRI) contrast agents for molecular imaging applications. *Acc Chem Res* **2009,** *42*, 822-31.

[33] Aime, S.; Castelli, D. D.; Terreno, E. Chapter 10 - Lanthanide-loaded paramagnetic liposomes as switchable magnetically oriented nanovesicles. *Methods Enzymol.* **2009,** *464*, 193-210.

[34] Burdinski, D.; Pikkemaat, J. A.; Emrullahoglu, M.; Costantini, F.; Verboom, W.; Langereis, S.; Grull, H.; Huskens, J. Targeted LipoCEST Contrast Agents for Magnetic Resonance Imaging: Alignment of Aspherical Liposomes on a Capillary Surface. *Angew. Chem. Int. Ed. Engl.*

[35] Merbach, A. E.; Tóth, E. *The Chemistry of Contrast Agents in Medical Resonance Imaging*. Wiley: Chichester, 2001.

[36] Krause, W. *Contrast Agents I: Magnetic Resonance Imaging*. Springer: Berlin, 2002; Vol. 221.

[37] Caravan, P.; Ellison, J. J.; McMurry, T. J.; Lauffer, R. B. Gadolinium(III) Chelates as MRI Contrast Agents: Structure, Dynamics, and Applications. *Chem. Rev.* **1999,** *99*, 2293-2352.

[38] Aime, S.; Barge, A.; Gianolio, E.; Pagliarin, R.; Silengo, L.; Tei, L. High relaxivity contrast agents for MRI and molecular imaging. *Ernst Schering Res. Found. Workshop* **2005**, 99-121.

[39] Aime, S.; Barge, A.; Cabella, C.; Crich, S. G.; Gianolio, E. Targeting cells with MR imaging probes based on paramagnetic Gd(III) chelates. *Curr. Pharm. Biotechnol.* **2004,** *5*, 509-18.

[40] Cai, W.; Chen, X. Nanoplatforms for targeted molecular imaging in living subjects. *Small* **2007,** *3*, 1840-54.

[41] Thorek, D. L.; Chen, A. K.; Czupryna, J.; Tsourkas, A. Superparamagnetic iron oxide nanoparticle probes for molecular imaging. *Ann. Biomed. Eng.* **2006,** *34*, 23-38.

[42] Cintra, E. R.; Ferreira, F. S.; Santos Junior, J. L.; Campello, J. C.; Socolovsky, L. M.; Lima, E. M.; Bakuzis, A. F. Nanoparticle agglomerates in magnetoliposomes. *Nanotechnology* **2009,** *20*, 45103.

[43] Toth, E.; Helm, L.; Merbach, A. E. Relaxivity of Gadolinium (III) complexes: Theory and mechanism. In *The Chemistry of Contrast Agents in Medical Magnetic Resonance Imaging*, Merbach, A. E. a. T., E., Ed. John Wiley and Sons: Chichester, 2002; pp 45-120.

[44] Idee, J. M.; Port, M.; Robic, C.; Medina, C.; Sabatou, M.; Corot, C. Role of thermodynamic and kinetic parameters in gadolinium chelate stability. *J. Magn. Reson. Imaging* **2009,** *30*, 1249-58.

[45] Sherry, A. D.; Caravan, P.; Lenkinski, R. E. Primer on gadolinium chemistry. *J. Magn. Reson. Imaging* **2009,** *30*, 1240-8.

[46] Canavese, C.; Mereu, M. C.; Aime, S.; Lazzarich, E.; Fenoglio, R.; Quaglia, M.; Stratta, P. Gadolinium-associated nephrogenic systemic fibrosis: the need for nephrologists' awareness. *J. Nephrol.* **2008,** *21*, 324-36.

[47] Stratta, P.; Canavese, C.; Aime, S. Gadolinium-enhanced magnetic resonance imaging, renal failure and nephrogenic systemic fibrosis/nephrogenic fibrosing dermopathy. *Curr. Med. Chem.* **2008,** *15*, 1229-35.

[48] Lauffer, R. B. Paramagnetic metal complexes as water proton relaxation agents for NMR imaging: theory and design. *Chem. Rev.* **1987,** *87*, 901-927.

[49] Garcia-Martín, M. L.; Ballesteros, P.; Cerdan, S. The metabolism of water in cells and tissues as detected by Magnetic Resonance methods. *Prog. Nucl. Mag. Res. Spec.* **1999,** *39*, 41-77.

[50] Henkelman, R. M.; Stanisz, G. J.; Graham, S. J. Magnetization transfer in MRI: a review. *NMR Biomed.* **2001,** *14*, 57-64.

[51] Forsén, S.; Hoffman, R. A. Study of moderately rapid chemical exchange reactions by means of nuclear magnetic resonance double resonance. *J. Che. Phys.* **1963,** *39*, 2892-2901.

[52] Nitz, W. R.; Reimer, P. Contrast mechanisms in MR imaging. *Eur. Radiol.* **1999,** *9*, 1032-46.

[53] Zhou, J.; Zijl, P. C. M. v. Chemical exchange saturation transfer imaging and spectroscopy. *Prog. Nucl. Mag. Res. Spec.* **2006,** *48*, 109-136.

[54] Zhou, J.; Lal, B.; Wilson, D. A.; Laterra, J.; van Zijl, P. C. Amide proton transfer (APT) contrast for imaging of brain tumors. *Magn. Reson. Med.* **2003,** *50*, 1120-6.

[55] Sun, P. Z.; Zhou, J.; Huang, J.; van Zijl, P. Simplified quantitative description of amide proton transfer (APT) imaging during acute ischemia. *Magn. Reson. Med.* **2007,** *57*, 405-10.

[56] Zhou, J.; Wilson, D. A.; Sun, P. Z.; Klaus, J. A.; Van Zijl, P. C. Quantitative description of proton exchange processes between water and endogenous and exogenous agents for WEX, CEST, and APT experiments. *Magn. Reson. Med.* **2004,** *51*, 945-52.

[57] Zhou, J.; Payen, J. F.; Wilson, D. A.; Traytsman, R. J.; van Zijl, P. C. Using the amide proton signals of intracellular proteins and peptide to detect pH effects in MRI. *Nat. Med.* **2003,** *9*, 1085-90.

[58] Ward, K. M.; Balaban, R. S. Determination of pH using water protons and chemical exchange dependent saturation transfer (CEST). *Magn. Reson. Med.* **2000,** *44*, 799-802.

[59] Ward, K. M.; Aletras, A. H.; Balaban, R. S. A new class of contrast agents for MRI based on proton chemical exchange dependent saturation transfer (CEST). *J. Magn. Reson.* **2000,** *143*, 79-87.

[60] Le Bihan, D. Looking into the functional architecture of the brain with diffusion MRI. *Nature* **2003,** *4*, 469-480.

[61] Le Bihan, D.; Manguin, J.-F.; Poupon, C.; Clark, C. A.; Pappatta, S.; Molko, N.; Chabriat, H. Diffusion Tensor Imaging: Concepts and Applications. *J. Mag. Res. Imag.* *13*, 534-546.

[62] Nucifora, P. G.; Verma, R.; Lee, S. K.; Melhem, E. R. Diffusion-tensor MR imaging and tractography: exploring brain microstructure and connectivity. *Radiology* **2007,** *245*, 367-84.

[63] Negri, V.; Cerpa, A.; Lopez-Larrubia, P.; Nieto-Charques, L.; Cerdan, S.; Ballesteros, P. Nanotubular Paramagnetic Probes as Contrast Agents for Magnetic Resonance Imaging Based on the Diffusion Tensor. *Angew Chem Int Ed Engl* **2010**.

[64] Gillies, R. J.; Raghunand, N.; Garcia-Martin, M. L.; Gatenby, R. A. pH imaging. A review of pH measurement methods and applications in cancers. *IEEE Eng. Med. Biol. Mag.* **2004,** *23*, 57-64.

[65] Gillies, R. J.; Ugurbil, K.; den Hollander, J. A.; Shulman, R. G. 31P NMR studies of intracellular pH and phosphate metabolism during cell division cycle of Saccharomyces cerevisiae. *Proc Natl Acad Sci U S A* **1981,** *78*, 2125-9.

[66] Gadian, D. G.; Radda, G. K. NMR studies of tissue metabolism. *Annu. Rev. Biochem.* **1981,** *50*, 69-83.

[67] DeFronzo, M.; Gillies, R. J. Characterization of methylphosphonate as a 31P NMR pH indicator. *J Biol Chem* **1987,** *262*, 11032-7.

[68] Bore, P. J.; Chan, L.; Gadian, D. G.; Radda, G. K.; Ross, B. D.; Styles, P.; Taylor, D. J. Noninvasive pHi measurements of human tissue using 31P-NMR. *Kroc Found. Ser.* **1981,** *15*, 527-35.

[69] Perez-Mayoral, E.; Negri, V.; Soler-Padros, J.; Cerdan, S.; Ballesteros, P. Chemistry of paramagnetic and diamagnetic contrast agents for Magnetic Resonance Imaging and Spectroscopy pH responsive contrast agents. *Eur J Radiol* **2008,** *67*, 453-8.

[70] Gil, S.; Zaderenzo, P.; Cruz, F.; Cerdan, S.; Ballesteros, P. Imidazol-1-ylalkanoic acids as extrinsic 1H NMR probes for the determination of intracellular pH, extracellular pH and cell volume. *Bioorg. Med. Chem.* **1994,** *2*, 305-14.

[71] Ljungkvist, A. S.; Bussink, J.; Kaanders, J. H.; van der Kogel, A. J. Dynamics of tumor hypoxia measured with bioreductive hypoxic cell markers. *Radiat. Res.* **2007,** *167*, 127-145.

[72] Padhani, A. R.; Krohn, K. A.; Lewis, J. S.; Alber, M. Imaging oxygenation of human tumours. *Eur. Radiol.* **2007,** *17*, 861-872.

[73] Chapman, J. D.; Engelhardt, E. L.; Stobbe, C. C.; Schneider, R. F.; Hanks, G. E. Measuring hypoxia and predicting tumor radioresistance with nuclear medicine assays. *Radiother. Oncol.* **1998,** *46*, 229-237.

[74] Koch, C. J. Measurement of absolute oxygen levels in cells and tissues using oxygen sensors and 2-nitroimidazole EF5. *Methods Enzymol.* **2002,** *352*, 3-31.

[75] Evans, S. M.; Judy, K. D.; Dunphy, I.; Jenkins, W. T.; Nelson, P. T.; Collins, R.; Wileyto, E. P.; Jenkins, K.; Hahn, S. M.; Stevens, C. W.; Judkins, A. R.; Phillips, P.; Geoerger, B.; Koch, C. J. Comparative measurements of hypoxia in human brain tumors using needle electrodes and EF5 binding. *Cancer Res.* **2004,** *64*, 1886-1892.

[76] Brezden, C. B.; Horn, L.; McClelland, R. A.; Rauth, A. M. Oxidative stress and 1-methyl-2-nitroimidazole cytotoxicity. *Biochem. Pharmacol.* **1998,** *56*, 335-344.

[77] Varghese, A. J.; Whitmore, G. F. Properties of 2-hydroxylaminoimidazoles and their implications for the biological effects of 2-nitroimidazoles. *Chem. Biol. Interact.* **1985,** *56*, 269-287.

[78] Bolton, J. L.; McClelland, R. A. Kinetics and mechanism of the decomposition in aqueous solutions of 2-(hydroxyamino)imidazoles. *J. Am. Chem. Soc.* **1989,** *111*, 8172-8181.

[79] Seddon, B. M.; Workman, P. The role of functional and molecular imaging in cancer drug discovery and development. *Br. J. Radiol.* **2003,** *76*, S128-S138.

[80] Ardenkjaer-Larsen, J. H.; Fridlund, B.; Gram, A.; Hansson, G.; Hansson, L.; Lerche, M. H.; Servin, R.; Thaning, M.; Golman, K. Increase in signal-to-noise ratio of > 10,000 times in liquid-state NMR. *Proc. Natl. Acad. Sci. USA* **2003,** *100*, 10158-63.

[81] Golman, K.; Ardenkjaer-Larsen, J. H.; Petersson, J. S.; Mansson, S.; Leunbach, I. Molecular imaging with endogenous substances. *Proc. Natl. Acad. Sci. USA* **2003,** *100*, 10435-9.

[82] Golman, K.; Zandt, R. I.; Lerche, M.; Pehrson, R.; Ardenkjaer-Larsen, J. H. Metabolic imaging by hyperpolarized 13C magnetic resonance imaging for in vivo tumor diagnosis. *Cancer Res.* **2006,** *66*, 10855-60.

[83] Kurhanewicz, J.; Bok, R.; Nelson, S. J.; Vigneron, D. B. Current and potential applications of clinical 13C MR spectroscopy. *J. Nucl. Med.* **2008,** *49*, 341-4.

[84] Mansson, S.; Johansson, E.; Magnusson, P.; Chai, C. M.; Hansson, G.; Petersson, J. S.; Stahlberg, F.; Golman, K. 13C imaging-a new diagnostic platform. *Eur. Radiol.* **2006,** *16*, 57-67.

[85] Comment, A.; Rentsch, J.; Kurdzesau, F.; Jannin, S.; Uffmann, K.; van Heeswijk, R. B.; Hautle, P.; Konter, J. A.; van den Brandt, B.; van der Klink, J. J. Producing over 100 ml of highly concentrated hyperpolarized solution by means of dissolution DNP. *J. Magn. Reson.* **2008,** *194*, 152-5.

[86] Yen, Y. F.; Kohler, S. J.; Chen, A. P.; Tropp, J.; Bok, R.; Wolber, J.; Albers, M. J.; Gram, K. A.; Zierhut, M. L.; Park, I.; Zhang, V.; Hu, S.; Nelson, S. J.; Vigneron, D. B.; Kurhanewicz, J.; Dirven, H. A.; Hurd, R. E. Imaging considerations for in vivo 13C metabolic mapping using hyperpolarized 13C-pyruvate. *Magn Reson Med* **2009,** *62*, 1-10.

[87] Schroeder, M. A.; Atherton, H. J.; Ball, D. R.; Cole, M. A.; Heather, L. C.; Griffin, J. L.; Clarke, K.; Radda, G. K.; Tyler, D. J. Real-time assessment of Krebs cycle metabolism using hyperpolarized 13C magnetic resonance spectroscopy. *FASEB J.* **2009,** *23*, 2529-38.

[88] Albers, M. J.; Bok, R.; Chen, A. P.; Cunningham, C. H.; Zierhut, M. L.; Zhang, V. Y.; Kohler, S. J.; Tropp, J.; Hurd, R. E.; Yen, Y. F.; Nelson, S. J.; Vigneron, D. B.; Kurhanewicz, J. Hyperpolarized 13C lactate, pyruvate, and alanine: noninvasive biomarkers for prostate cancer detection and grading. *Cancer Res.* **2008,** *68*, 8607-15.

[89] Gallagher, F. A.; Kettunen, M. I.; Day, S. E.; Hu, D. E.; Ardenkjaer-Larsen, J. H.; Zandt, R.; Jensen, P. R.; Karlsson, M.; Golman, K.; Lerche, M. H.; Brindle, K. M. Magnetic resonance imaging of pH in vivo using hyperpolarized 13C-labelled bicarbonate. *Nature* **2008,** *453*, 940-3.

[90] Schroeder, M. A.; Swietach, P.; Atherton, H. J.; Gallagher, F. A.; Lee, P.; Radda, G. K.; Clarke, K.; Tyler, D. J. Measuring intracellular pH in the heart using hyperpolarized carbon dioxide and bicarbonate: a 13C and 31P magnetic resonance spectroscopy study. *Cardiovasc. Res.*

[91] Bruce, J. I.; Dickins, R. S.; Govenlock, L. J.; Gunnlaugsson, T.; Lopinski, S.; Lowe, M. P.; Parker, D.; Peacock, R. D.; Perry, J. J. B.; Aime, S.; Botta, M. The Selectivity of Reversible Oxy-Anion Binding in Aqueous Solution at a Chiral Europium and Terbium Center: Signaling of Carbonate Chelation by Changes in the Form and Circular Polarization of Luminescence Emission. *J. Am. Chem. Soc.* **2000,** *122*, 9674-9684.

[92] Zhang, S.; Wu, K.; Sherry, A. D. A Novel pH-Sensitive MRI Contrast Agent. *Angew. Chem. Int. Ed. Engl.* **1999,** *38*, 3192-3194.

[93] Garcia-Martin, M. L.; Martinez, G. V.; Raghunand, N.; Sherry, A. D.; Zhang, S.; Gillies, R. J. High resolution pH(e) imaging of rat glioma using pH-dependent relaxivity. *Magn. Reson. Med.* **2006,** *55*, 309-15.

[94] Raghunand, N.; Howison, C.; Sherry, A. D.; Zhang, S.; Gillies, R. J. Renal and systemic pH imaging by contrast-enhanced MRI. *Magn. Reson. Med.* **2003,** *49*, 249-57.

[95] Raghunand, N.; Zhang, S.; Sherry, A. D.; Gillies, R. J. In vivo magnetic resonance imaging of tissue pH using a novel pH-sensitive contrast agent, GdDOTA-4AmP. *Acad. Radiol.* **2002,** *9 Suppl 2*, S481-3.

[96] Aime, S.; Fedeli, F.; Sanino, A.; Terreno, E. A R2/R1 ratiometric procedure for a concentration-independent, pH-responsive, Gd(III)-based MRI agent. *J. Am. Chem. Soc.* **2006,** *128*, 11326-7.

[97] Aime, S.; Barge, A.; Botta, M.; Howard, J. A. K.; Kataky, R.; Lowe, M. P.; Moloney, J. M.; Parker, D.; de Sousa, A. S. Dependence of the relaxivity and luminescence of gadolinium and europium amino-acid complexes on hydrogencarbonate and pH. *Chem. Commun.* **1999**, 1047 - 1048.

[98] Terreno, E.; Botta, M.; Dastru, W.; Aime, S. Gd-enhanced MR images of substrates other than water. *Contrast Media Mol. Imaging* **2006,** *1*, 101-5.

[99] Aime, S.; Barge, A.; Delli Castelli, D.; Fedeli, F.; Mortillaro, A.; Nielsen, F. U.; Terreno, E. Paramagnetic lanthanide(III) complexes as pH-sensitive chemical exchange saturation transfer (CEST) contrast agents for MRI applications. *Magn. Reson. Med.* **2002,** *47*, 639-48.

[100] Aime, S.; Delli Castelli, D.; Fedeli, F.; Terreno, E. A paramagnetic MRI-CEST agent responsive to lactate concentration. *J. Am. Chem. Soc.* **2002,** *124*, 9364-5.

[101] Zhang, S.; Merritt, M.; Woessner, D. E.; Lenkinski, R. E.; Sherry, A. D. PARACEST agents: modulating MRI contrast via water proton exchange. *Acc. Chem. Res.* **2003,** *36*, 783-90.

[102] Terreno, E.; Stancanello, J.; Longo, D.; Castelli, D. D.; Milone, L.; Sanders, H. M.; Kok, M. B.; Uggeri, F.; Aime, S. Methods for an improved detection of the MRI-CEST effect. *Contrast Media Mol. Imaging* **2009,** *4*, 237-47.

[103] Helm, L.; Merbach, A. E. Inorganic and bioinorganic solvent exchange mechanisms. *Chem. Rev.* **2005,** *105*, 1923-59.

[104] Trokowski, R.; Zhang, S.; Sherry, A. D. Cyclen-based phenylboronate ligands and their Eu3+ complexes for sensing glucose by MRI. *Bioconj. Chem.* **2004,** *15*, 1431-40.

[105] Ren, J.; Trokowski, R.; Zhang, S.; Malloy, C. R.; Sherry, A. D. Imaging the tissue distribution of glucose in livers using a PARACEST sensor. *Magn. Reson. Med.* **2008,** *60*, 1047-55.

[106] Chang, Y. T.; Cheng, C. M.; Su, Y. Z.; Lee, W. T.; Hsu, J. S.; Liu, G. C.; Cheng, T. L.; Wang, Y. M. Synthesis and characterization of a new bioactivated paramagnetic gadolinium(III) complex [Gd(DOTA-FPG)(H2O)] for tracing gene expression. *Bioconj. Chem.* **2007,** *18*, 1716-27.

[107] Zhang, S.; Malloy, C. R.; Sherry, A. D. MRI thermometry based on PARACEST agents. *J Am Chem Soc* **2005,** *127*, 17572-3.

[108] Li, A. X.; Wojciechowski, F.; Suchy, M.; Jones, C. K.; Hudson, R. H.; Menon, R. S.; Bartha, R. A sensitive PARACEST contrast agent for temperature MRI: Eu3+-DOTAM-glycine (Gly)-phenylalanine (Phe). *Magn. Reson. Med.* **2008,** *59*, 374-81.

[109] Gilad, A. A.; Ziv, K.; McMahon, M. T.; van Zijl, P. C.; Neeman, M.; Bulte, J. W. MRI reporter genes. *J Nucl Med* **2008,** *49*, 1905-8.

[110] Louie, A. Y.; Huber, M. M.; Ahrens, E. T.; Rothbacher, U.; Moats, R.; Jacobs, R. E.; Fraser, S. E.; Meade, T. J. In vivo visualization of gene expression using magnetic resonance imaging. *Nat Biotechnol* **2000,** *18*, 321-5.

[111] Hanaoka, K.; Kikuchi, K.; Terai, T.; Komatsu, T.; Nagano, T. A Gd3+-based magnetic resonance imaging contrast agent sensitive to beta-galactosidase activity utilizing a receptor-induced magnetization enhancement (RIME) phenomenon. *Chemistry* **2008,** *14*, 987-95.

[112] Genove, G.; DeMarco, U.; Xu, H.; Goins, W. F.; Ahrens, E. T. A new transgene reporter for in vivo magnetic resonance imaging. *Nat Med* **2005,** *11*, 450-4.

[113] Goldhawk, D. E.; Lemaire, C.; McCreary, C. R.; McGirr, R.; Dhanvantari, S.; Thompson, R. T.; Figueredo, R.; Koropatnick, J.; Foster, P.; Prato, F. S. Magnetic resonance imaging of cells overexpressing MagA, an endogenous contrast agent for live cell imaging. *Mol Imaging* **2009,** *8*, 129-39.

[114] Zhang, C. Y.; Lu, J.; Tsourkas, A. Iron chelator-based amplification strategy for improved targeting of transferrin receptor with SPIO. *Cancer Biol Ther* **2008,** *7*, 889-95.

[115] Garcia-Martin, M. L.; Herigault, G.; Remy, C.; Farion, R.; Ballesteros, P.; Coles, J. A.; Cerdan, S.; Ziegler, A. Mapping extracellular pH in rat brain gliomas in vivo by 1H magnetic resonance spectroscopic imaging: comparison with maps of metabolites. *Cancer Res* **2001,** *61*, 6524-31.

[116] Provent, P.; Benito, M.; Hiba, B.; Farion, R.; Lopez-Larrubia, P.; Ballesteros, P.; Remy, C.; Segebarth, C.; Cerdan, S.; Coles, J. A.; Garcia-Martin, M. L. Serial in vivo spectroscopic nuclear magnetic resonance imaging of lactate and extracellular pH in rat gliomas shows redistribution of protons away from sites of glycolysis. *Cancer Res* **2007,** *67*, 7638-45.

[117] Varghese, A. J.; Gulyas, S.; Mohindra, J. K. Hypoxia-dependent reduction of 1-(2-nitro-1-imidazolyl)-3-methoxy-2-propanol by Chinese hamster ovary cells and KHT tumor cells in vitro and in vivo. *Cancer Res.* **1976,** *36*, 3761-3765.

[118] Raleigh, J. A.; Franko, A. J.; Treiber, E. O.; Lunt, J. A.; Allen, P. S. Covalent binding of a fluorinated 2-nitroimidazole to EMT-6 tumors in Balb/C mice: detection by F-19 nuclear magnetic resonance at 2.35 T. *Int. J. Radiat. Oncol. Biol. Phys.* **1986,** *12*, 1243-1245.

[119] Raleigh, J. A.; Franko, A. J.; Kelly, D. A.; Trimble, L. A.; Allen, P. S. Development of an in vivo 19F magnetic resonance method for measuring oxygen deficiency in tumors. *Magn Reson.Med.* **1991,** *22*, 451-466.

[120] Aboagye, E. O.; Lewis, A. D.; Tracy, M.; Workman, P. Bioreductive metabolism of the novel fluorinated 2-nitroimidazole hypoxia probe N-(2-hydroxy-3,3,3-trifluoropropyl)-2-(2-nitroimidazolyl) acetamide (SR-4554). *Biochem. Pharmacol.* **1997,** *54*, 1217-1224.

[121] Aboagye, E. O.; Maxwell, R. J.; Kelson, A. B.; Tracy, M.; Lewis, A. D.; Graham, M. A.; Horsman, M. R.; Griffiths, J. R.; Workman, P. Preclinical evaluation of the fluorinated 2-nitroimidazole N-(2-hydroxy-3,3,3-trifluoropropyl)-2-(2-nitro-1-imidazolyl) acetamide (SR-4554) as a probe for the measurement of tumor hypoxia. *Cancer Res.* **1997,** *57*, 3314-3318.

[122] Aboagye, E. O.; Lewis, A. D.; Graham, M. A.; Tracy, M.; Kelson, A. B.; Ryan, K. J.; Workman, P. The pharmacokinetics, bioavailability and biodistribution in mice of a rationally designed 2-nitroimidazole hypoxia probe SR-4554. *Anticancer. Drug Des.* **1996,** *11*, 231-242.

[123] Seddon, B. M.; Maxwell, R. J.; Honess, D. J.; Grimshaw, R.; Raynaud, F.; Tozer, G. M.; Workman, P. Validation of the fluorinated 2-nitroimidazole SR-4554 as a noninvasive hypoxia marker detected by magnetic resonance spectroscopy. *Clin. Cancer Res.* **2002,** *8*, 2323-2335.

[124] Seddon, B. M.; Payne, G. S.; Simmons, L.; Ruddle, R.; Grimshaw, R.; Tan, S.; Turner, A.; Raynaud, F.; Halbert, G.; Leach, M. O.; Judson, I.; Workman, P. A phase I study of SR-4554 via intravenous administration for noninvasive investigation of tumor hypoxia by magnetic resonance spectroscopy in patients with malignancy. *Clin. Cancer Res.* **2003,** *9*, 5101-5112.

[125] Procissi, D.; Claus, F.; Burgman, P.; Koziorowski, J.; Chapman, J. D.; Thakur, S. B.; Matei, C.; Ling, C. C.; Koutcher, J. A. In vivo 19F magnetic resonance spectroscopy and chemical shift imaging of tri-fluoro-nitroimidazole as a potential hypoxia reporter in solid tumors. *Clin. Cancer Res.* **2007,** *13*, 3738-3747.

[126] Day, S. E.; Kettunen, M. I.; Gallagher, F. A.; Hu, D. E.; Lerche, M.; Wolber, J.; Golman, K.; Ardenkjaer-Larsen, J. H.; Brindle, K. M. Detecting tumor response to treatment using hyperpolarized 13C magnetic resonance imaging and spectroscopy. *Nat Med* **2007,** *13*, 1382-7.

[127] Schroeder, M. A.; Swietach, P.; Atherton, H. J.; Gallagher, F. A.; Lee, P.; Radda, G. K.; Clarke, K.; Tyler, D. J. Measuring intracellular pH in the heart using

hyperpolarized carbon dioxide and bicarbonate: a 13C and 31P magnetic resonance spectroscopy study. *Cardiovasc Res*.

[128] Merritt, M. E.; Harrison, C.; Storey, C.; Jeffrey, F. M.; Sherry, A. D.; Malloy, C. R. Hyperpolarized 13C allows a direct measure of flux through a single enzyme-catalyzed step by NMR. *Proc Natl Acad Sci U S A* **2007,** *104*, 19773-7.

[129] Moreno, K. X.; Sabelhaus, S. M.; Merritt, M. E.; Sherry, A. D.; Malloy, C. R. Competition of Pyruvate with Physiological Substrates for Oxidation by the Heart: Implications for Studies with Hyperpolarized [1-13C]Pyruvate. *Am J Physiol Heart Circ Physiol*.

[130] Padhani, A.; Krohn, K.; Lewis, J.; Alber, M. Imaging oxygenation of human tumours. *European radiology* **2007,** *17*, 861-872.

[131] Ljungkvist, A. S. E.; Bussink, J.; Kaanders, J. H. A. M.; van der Kogel, A. Dynamics of tumor hypoxia measured with bioreductive hypoxic cell markers. *Radiation Research* **2007,** *167*, 127-145.

[132] Procissi, D.; Claus, F.; Burgman, P.; Koziorowski, J.; Chapman, J. D.; Thakur, S.; Matei, C.; Ling, C. C.; Koutcher, J. In vivo 19F magnetic resonance spectroscopy and chemical shift imaging of tri-fluoro-nitroimidazole as a potential hypoxia reporter in solid tumors. *Clinical cancer research* **2007,** *13*, 3738-3747.

FIGURE LEGENDS

Fig. (1). The extracellular microenvironment of tissues (light blue) is located between the vascular (red) and intracellular (grey) spaces. A: Under normal conditions (A) it is characterized by relatively low concentrations of lactate and H^+ due to the efficient removal of these metabolic products by the microvasculature. B: Reduced performance of the microvasculature (purple) under most pathological situations results in lactate and H^+ accumulation among other waste products in the diseased extravascular space (brown). This review describes the different approaches developed to progress from conventional anatomical T_2 weighted MR images (inset A) to molecular images revealing particular properties of the extracellular environment as pH in the brain of rat bearing a C6 tumor (inset B).

Fig. (2). Fundamentals of paramagnetic water relaxation induced by Gd(III) chelates. The ccordination envelope of cyclen ligands occupy eight (1-8) of the nine coordination sites from Gd(III), allowing a single water molecule to enter the vacant site of the metal. Under these conditions, the T_1 of the coordinated water molecule is reduced to T_{1m}, this molecule being able to exchange with the solvent with an exchange rate k_{ex} and experience then Brownian diffusion (ADC). The ability of the complex to induce faster water relaxation rates $r_{1,2,2*}$ (known as relaxivities) may be improved by increasing the number of coordinated water molecules (q>1), slowing down the rotational correlation timer of the complex (τ_R) through binding to macromolecular carriers, or increasing the exchange rate k_{ex} between the solvent and the first coordination sphere. Faster ADC improves the amplification of the inner sphere relaxivity effects.

Fig. (3). Magnetization Transfer Contrast. Tissue water may be present primarily in two different environments, “bound” (dark blue) as solvation water to different biomolecues (BM) or “free” (light blue) as solvent. Water molecules exchange (k_{ex}) between these two environments (A). Saturating the “bound water” resonance with an selective Rf pulse (R_f) results in a decrease of the original water resonance from (M_o) to (M_{sat}), because the saturated spins are transferred to the solvent (B). This exchange is influenced by additional environmental factors including temperature, pH and the Apparent Diffusion Coefficient (ADC). Lower panels: Representative saturation transfer images from rat bearing a C6 grioma; (C) T2 weighted image before the saturation pulse, (D) after the saturation pulse and (E) Magnetization Transfer M_{sat}/M_o map.

Fig. (4). In vivo measurements of the Apparent Diffusion Coefficient (ADC) by in vivo MRI allow to probe tissue microstructure. A: The classical Stejstahl-Tanner sequence. δ: duration of the diffusion encoding gradient. Δ: Diffusion measurement time. Pixel by pixel measurements of the signal intensities obtained for increasing diffusion gradient values allow the determination of the pixel by pixel ADC map of a representative rat brai bearing a C6 glioma (D). During the same Δ_{diff} tissue water will diffuse longer paths in less cellularly crowded (B) than in more cellularly crowded environments (C).

Fig. (5). Imidazolic pO_2 probes. A: Some imidazole derivatives currently used as oxygen probes by PET (^{18}F-Fluoromisonidazol), optical methods (Pimonidazol) and ^{19}FMRI/MRS (EF5 and TF-MISO). B: Comparison of PET images from the uptake of FDG glucose (left) or ^{18}F-Fluoromisonidazol (right). Note that only one of the nodules positive to FDG is hypoxic as revealed by F-MISO. C: Fluorescence micrograph from a head and neck squamous carcinoma showing pimonidazol accumulation in the hypoxic areas (green) surrounding the necrotic core. D: Retention maps of TF-MISO as detected by ^{19}F MRSI showing hypoxic areas (right inset) and ^{19}F spectra showing the accumulation of TF-MISO only in the hypoxic zones (left inset). Illustrations are taken from refs [130], [131] and [132] and reproduced with permission of the publisher.

Fig. (6). Structures of ligands derived from the cyclen structure useful as pH sensors using relaxivity enhancement (A and B) or PARACEST methods (C).

Fig. (7). Structures of imidazolic derivatives currently used as extracellular pH probes.

Fig. (8). Extracellular pH maps obtained with IEPA from implanted C6 gliomas. A and B: ^{1}H NMR PRESS spectra from the contralateral and ipsilateral hemispheres. Note that IEPA only accumulated in the tumor. C: Gd(III) DOTA enhanced image of the same C6 tumor showing peripheral enhancement of the vascularised regions. D: ^{1}H MRSI image of IEPA accumulation in the tumor. E. Titration of the pH dependence of the imidazolic H2 proton from IEPA. F: Extracellular pH map obtained from the chemical shift of IEPA H2 resonance observed in the tumor. Reproduced from ref. [115] with permission of the publisher.

Fig. (9). Imaging the tumor pH in vivo by ^{13}C MRSI using hyperpolarized $^{13}CO_3H^-/CO_2$. A: T_2 weighted image showing the EL4 tumor localization B: pH map calculated from the intensity maps of HCO_3^- (C) and CO_2 (D). Reproduced from ref [126] with permission of the publisher.

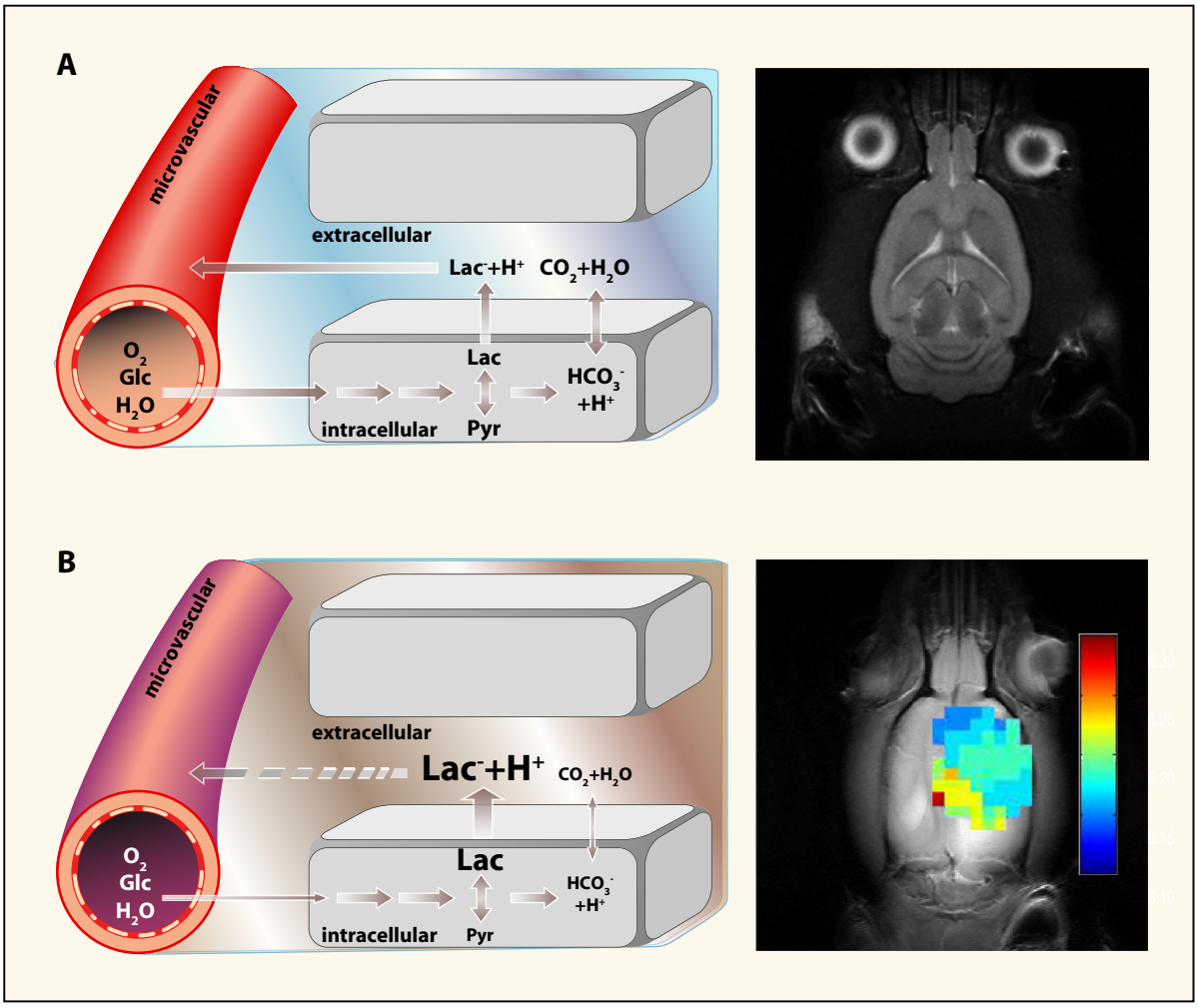

Figure 1
Pacheco et al.

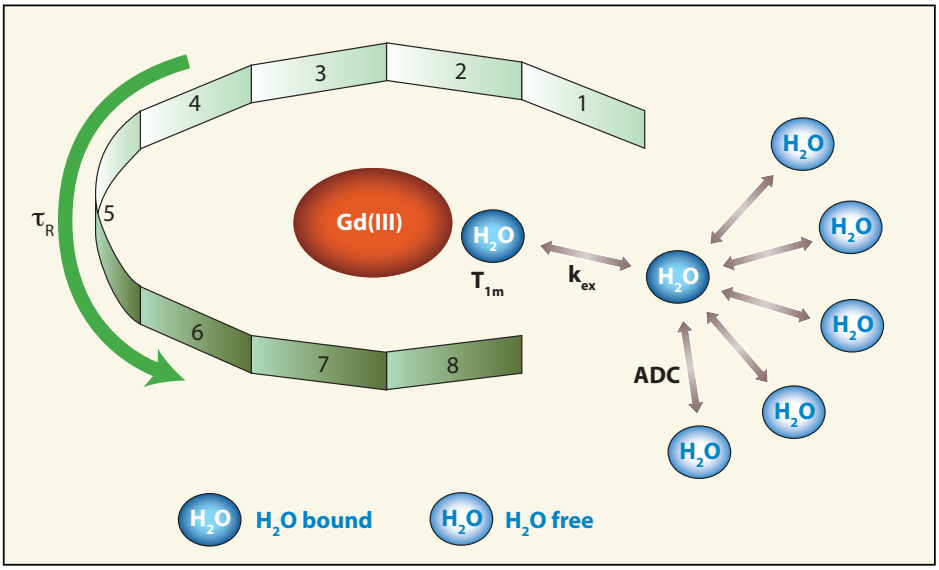

Figure 2
Pacheco et al.

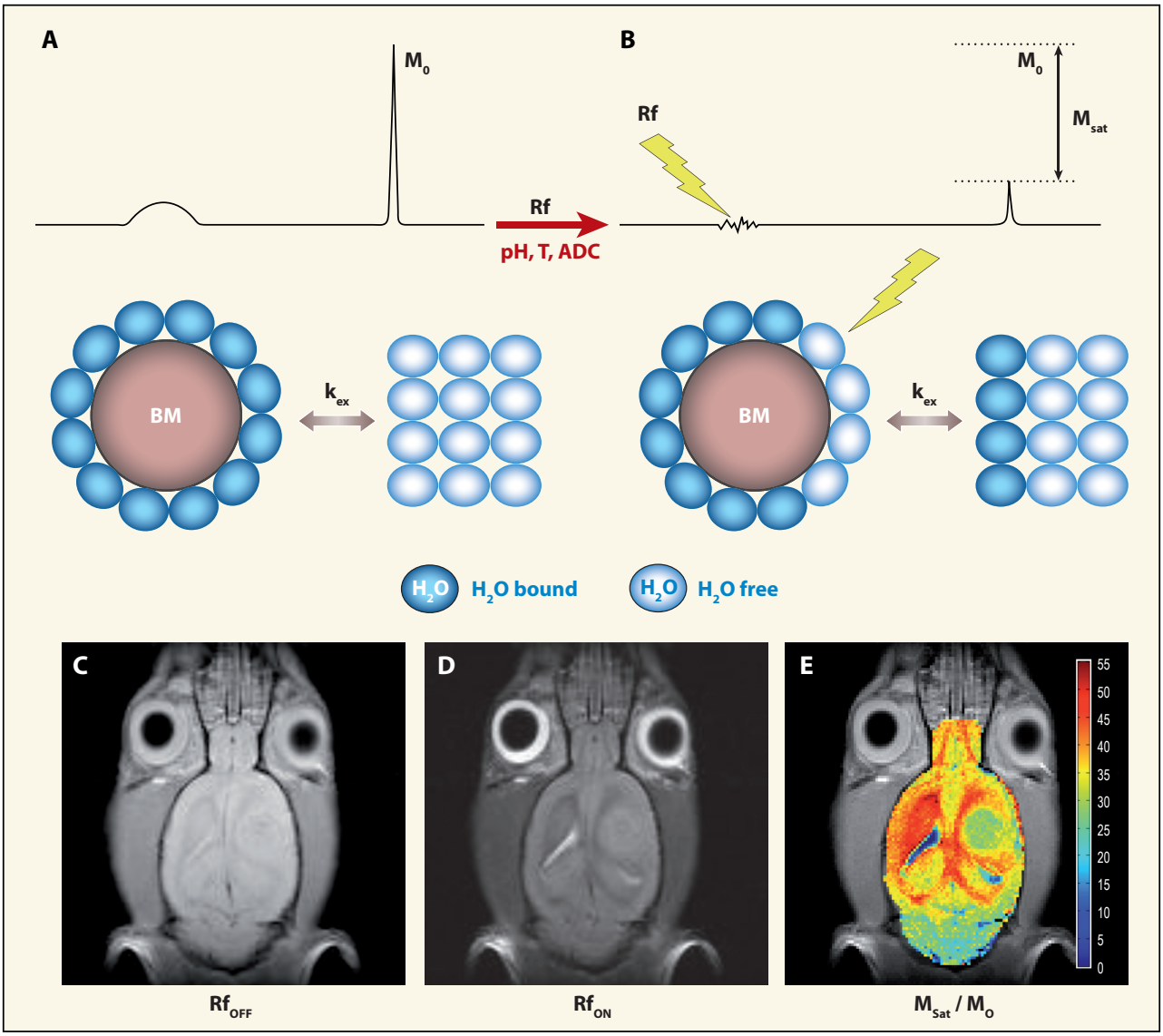

Figure 3
Pacheco et al.

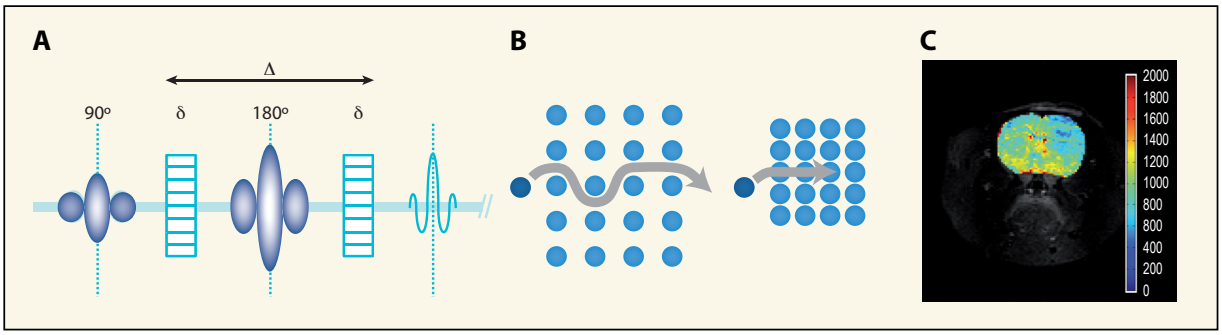

Figure 4
Pacheco et al.

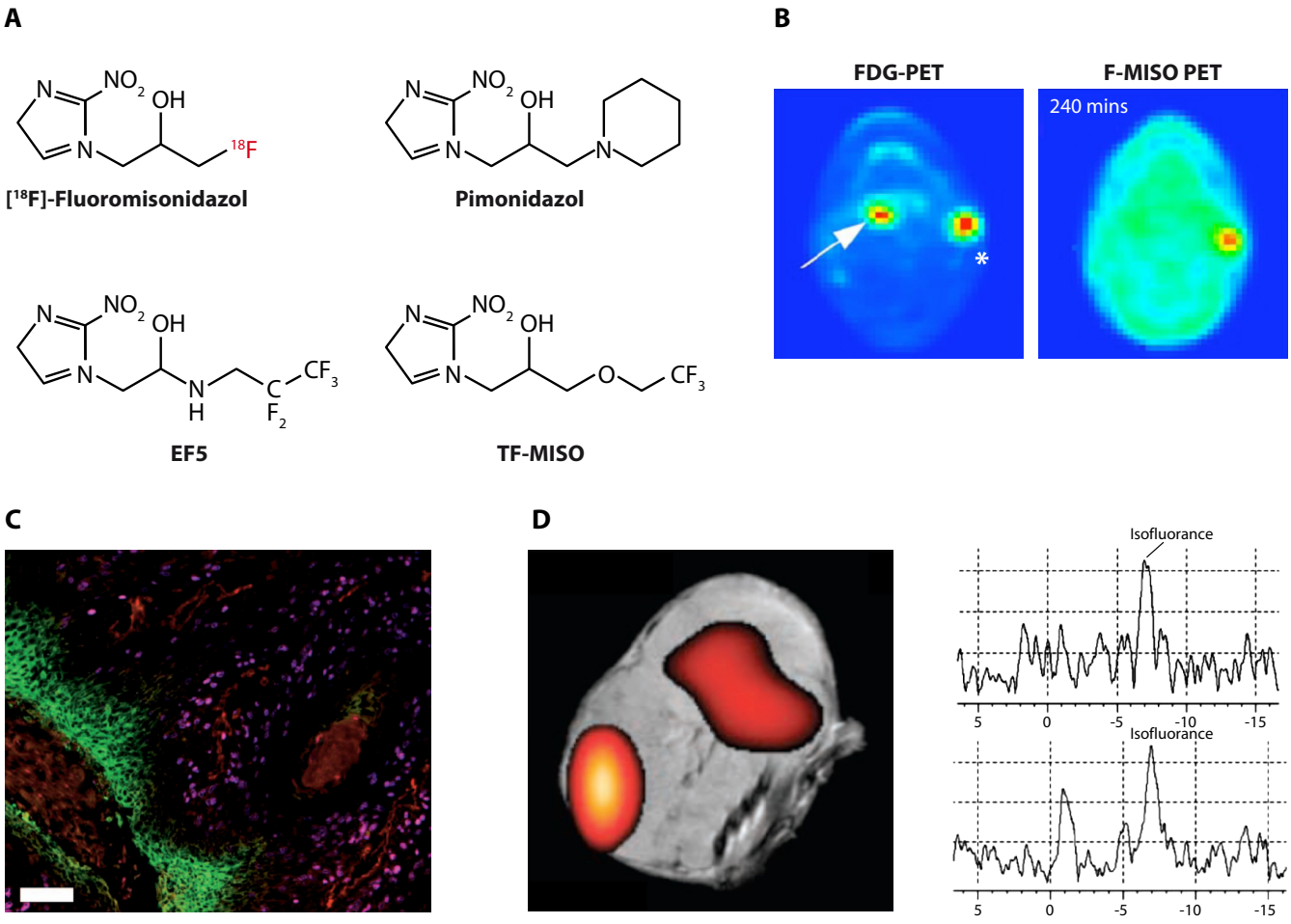

Figure 5
Pacheco et al.

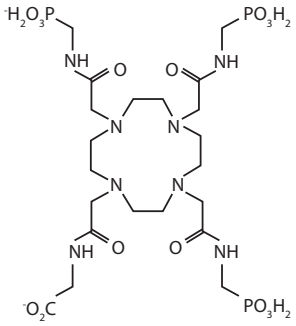

DOTAM-MP

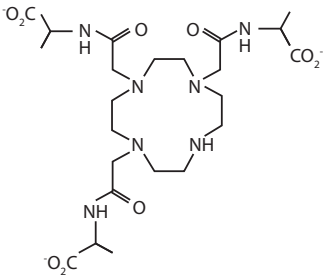

DO3A-Ala

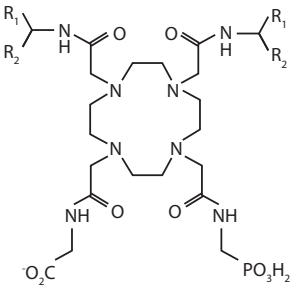

DOTAM-MP

1: $R_1 = H$, $R_2 = H$
2: $R_1 = H$, $R_2 = CH_2CO_2Et$
3: $R_1 = H$, $R_2 = CH_2CO_2$

Figure 6
Pacheco et al.

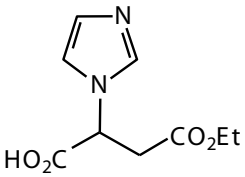

IEPA

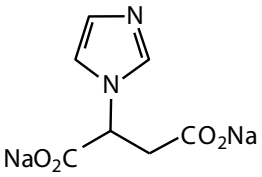

ISUCA

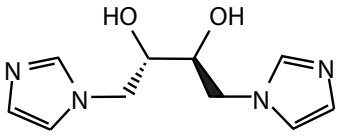

DIMOL-1

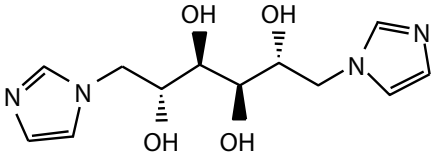

DIMOL-2

Figure 7
Pacheco et al.

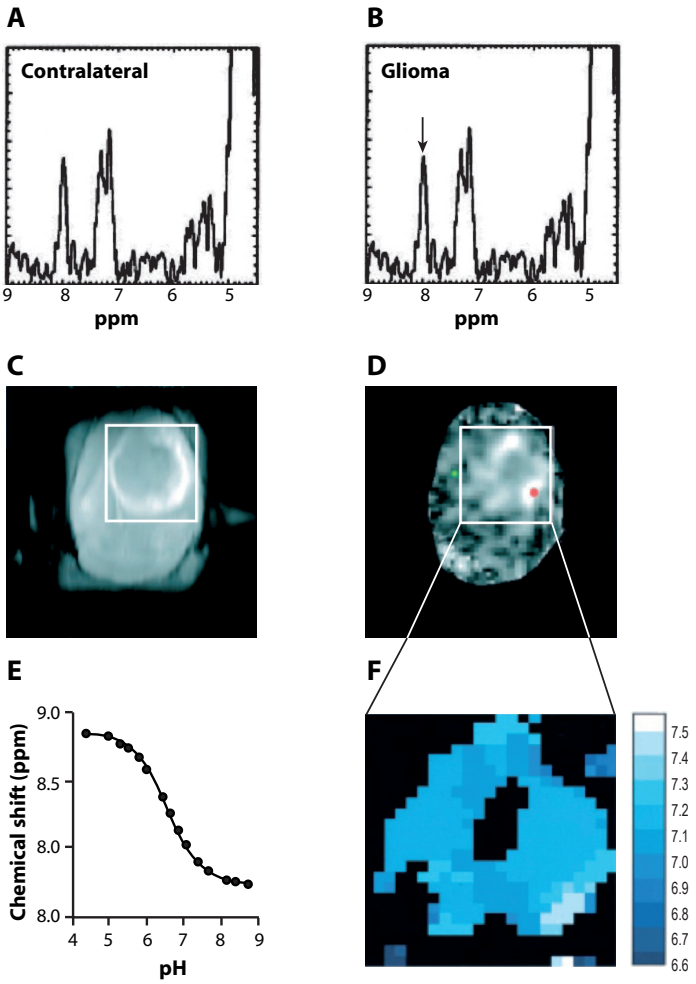

Figure 8
Pacheco et al.

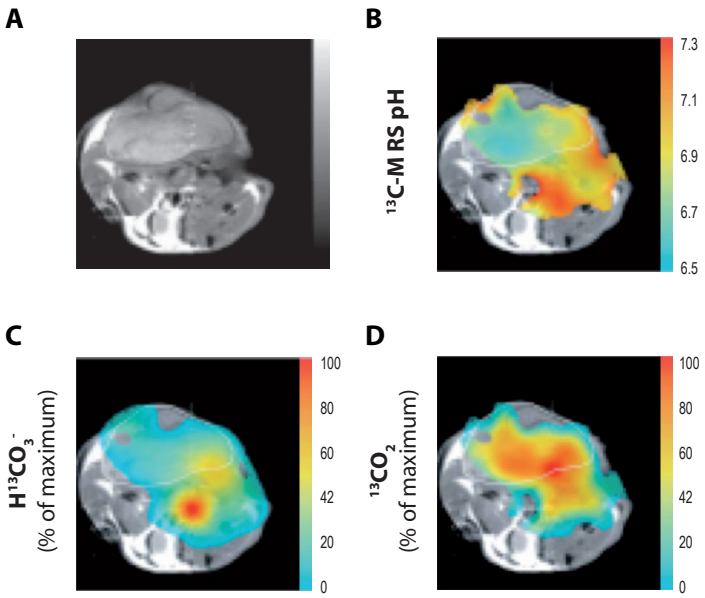

Figure 9_1
Pacheco et al.